ELSEVIER

Journal of Alloys and Compounds 463 (2008) 92–95

Journal of ALLOYS AND COMPOUNDS

www.elsevier.com/locate/jallcom

Low-temperature synthesis and characterization of ZnO quantum dots

Lili Yang [a,b,c], Jinghai Yang [a,c,*], Xiaoyan Liu [c], Yongjun Zhang [c], Yaxin Wang [c], Hougang Fan [c], Dandan Wang [a,b,c], Jihui Lang [c]

[a] *Key Laboratory of Excited State Processes, Changchun Institute of Optics, Fine Mechanics and Physics, Chinese Academy of Sciences, Changchun 130033, People's Republic of China*

[b] *Graduate School of the Chinese Academy of Sciences, Beijing 100049, People's Republic of China*

[c] *Institute of Condensed State Physics, Jilin Normal University, Siping 136000, People's Republic of China*

Received 13 November 2007; received in revised form 2 December 2007; accepted 3 December 2007
Available online 8 December 2007

Abstract

ZnO quantum dots (QDs) were fabricated at low temperature of 200 °C through thermal decomposition method with slight introduction of sodium dodecyl sulfate (SDS). The morphology, structure and optical properties were investigated by the methods of X-ray diffraction (XRD), transmission electron microscope (TEM), photoluminescence (PL) and Raman spectrum, respectively. The XRD results showed the as-synthesized ZnO QDs had hexagonal wurtzite structure and the average grain size estimated from Scherrer formula was 7.5 nm which had a good agreement with TEM result. And it is evident that the introduction of SDS can actually decrease the grain size to form ZnO QDs. The Raman results also indicated that the ZnO QDs keep the overall crystal structure of the bulk ZnO. Both spatial confinement within the dot boundaries and phonon localization by defects were the mainly reason for the only few cm^{-1} redshift of the Raman scatter peaks. The room-temperature photoluminescence reveals that the as-prepared ZnO QDs exhibit an ultraviolet emission at 380 nm and a broad deep level emission band in the range of 420–700 nm in wavelength, which testified the Raman and XRD results that the as-synthesized ZnO QDs had defects. Moreover, the growth mechanism of ZnO QDs was also discussed in the article.

Keywords: Semiconductors; Crystal structure; Optical spectroscopy

1. Introduction

Zinc oxide (ZnO) as one of the most important semiconductor has attracted significant attention in recent years. Compared to other wide band-gap materials, ZnO is a direct band-gap wurtzite-type semiconductor with band-gap energy of 3.37 eV at room temperature. Due to the extreme large exciton binding energy (about 60 meV), the excitons in ZnO are thermally stable at room temperature, and thus ZnO has significant advantages in optoelectronic applications such as in the ultraviolet (UV) lasing media laser diodes, varistors, sensors, transducers and photovoltaic devices [1–3]. For the feasible requirement, low-dimensional ZnO nanostructures, such as quantum dots (QDs) [4,5], nanoparticles (NPs) [6,7], nanobelts [7,8], nanowires [9] and quantum wells [10], have been widely investigated. In particular, ZnO QDs are of great interest because that the three-dimensional confinement of carrier and phonon leads not only continuous tuning of the optoelectronic properties but also improvement in device performance. The special application advantages of ZnO QDs and NPs in the area of bioscience also improve more attention due to its "survival lifetime" of a few hours, the slow solubility and high compatibility in biofluid and necessaries of Zn for human beings everyday [11]. Therefore, a number of reports of fabrication, structural, and optical characterization of ZnO QDs have been done in recent years [12–18].

So far, various physical or chemical synthetic approaches have been developed to fabricate QDs, such as vapor phase transport process [12], metal-organic chemical-vapor deposition (MOCVD) [13,14], RF magnetron sputtering [15], ion implantation [16], precipitation [17] and flame spray pyrolysis [18]. According to these methods, the complex processes, sophisticated equipment and economically prohibitive high tem-

* Corresponding author at: Institute of Condensed State Physics, Jilin Normal University, Siping 136000, People's Republic of China. Tel.: +86 434 3290009; fax: +86 434 3294566.
E-mail address: jhyang1@jlnu.edu.cn (J. Yang).

0925-8388/$ – see front matter © 2007 Elsevier B.V. All rights reserved.
doi:10.1016/j.jallcom.2007.12.006

peratures are usually required, which decides they are not suitable for large-scale fabrication with a relatively low cost. In this paper, a simple thermal decomposition method was used to obtain ZnO QDs. The most important thing is that the experiment can be carried out under low temperature of 200 °C. Moreover, the structure and photoluminescence of ZnO QDs have also been investigated in details.

2. Experimental

In our experiments, all chemicals were analytical reagent grade and used without further purification. Stoichiometric NH_4HCO_3, $ZnCl_2$ and slight sodium dodecyl sulfate ($C_{12}H_{25}NaO_4S$) (SDS) were dissolved in distilled water, respectively. The solution of NH_4HCO_3 and SDS were firstly mixed together in one beaker. And then $ZnCl_2$ solution was added into this mixed solution drop by drop. During the dropping process, white precipitations were gradually formed in the solution. After dropping, the filtered white precipitations were washed with alcohol for several times and then dried in the oven at 50–60 °C for 3–4 h, which formed the precursor of the ZnO QDs. Finally, ZnO quantum dots with a light yellow color were obtained after annealing at 200 °C for 1 h in air. Two samples were synthesized in our experiments. The mole ratio between SDS and $ZnCl_2$ is (a) 0 and (b) 0.0001, respectively.

X-ray diffraction (XRD) (MAC Science, MXP18, Japan), transmission electron microscope (TEM) (200 keV, JEM-2100HR, Japan), photoluminescence (PL) and Raman spectrometer were used to investigate the structure and optical properties of as-synthesized ZnO QDs. He–Cd laser with 325 nm emission was used for PL excitation. A Bruker RFS100/S FT-Raman spectrometer with a Nd–yttirium–aluminium garnet laser source (1064 nm, 500 mW) was used for recording Raman spectra of the samples.

3. Results and discussion

XRD was used to identify the crystal phase of the as-prepared samples. The XRD spectra of the samples were shown in Fig. 1. It can be seen that all the diffraction peaks could be identified to ZnO peaks compared with the standard card of bulk ZnO with hexagonal wurtzite structure (JCPDS No. 800075) and there were no diffraction peaks of other impurities, which indicated the as-synthesized sample was single phase of ZnO with hexagonal wurtzite structure. It is obvious that the diffraction peaks of the sample (b) are much broader than that of the sample (a). In the diffraction pattern, peak broadening is mainly

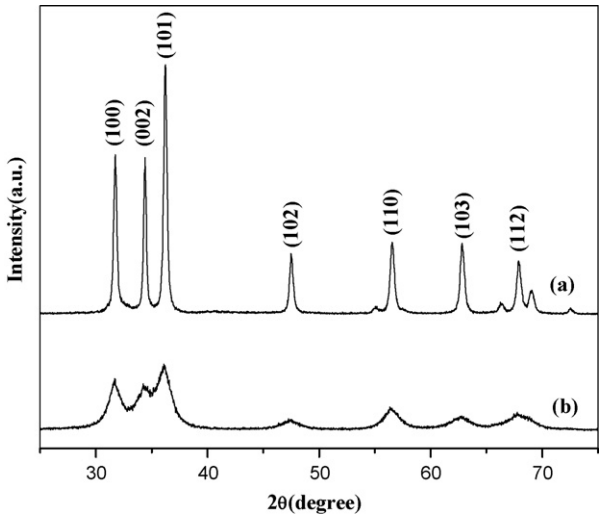

Fig. 1. XRD spectra of the samples (a) and (b).

due to four factors: microstrains (deformations of the lattice), faulting (extended defects), crystalline domain size and domain size distribution [19]. If we assume that the analyzed fine ZnO samples are free of strains and faulting, the peak broadening is only due to the crystalline domain size. Then the crystalline domain size can be calculated from Scherrer formula, which can be described as follows [19]:

$$D = \frac{0.89\lambda}{B\cos\theta} \quad (1)$$

where D is the grain size, λ the X-ray wavelength(0.15406 nm), θ the Bragg diffraction angle, and B is the peak width at half maximum (FWHM). The grain sizes of our samples were calculated with the (1 0 1) diffraction peak. The grain size of samples (a) and (b) was 27.2 and 7.5 nm, respectively. In order to clearly seen the grain size, TEM was used to characterize the samples. Fig. 2 shows the lower magnification and high-resolution TEM images. From Fig. 2, it can be seen that the average grain size of sample (b) was about 8 nm, which testified the estimated results from XRD pattern.

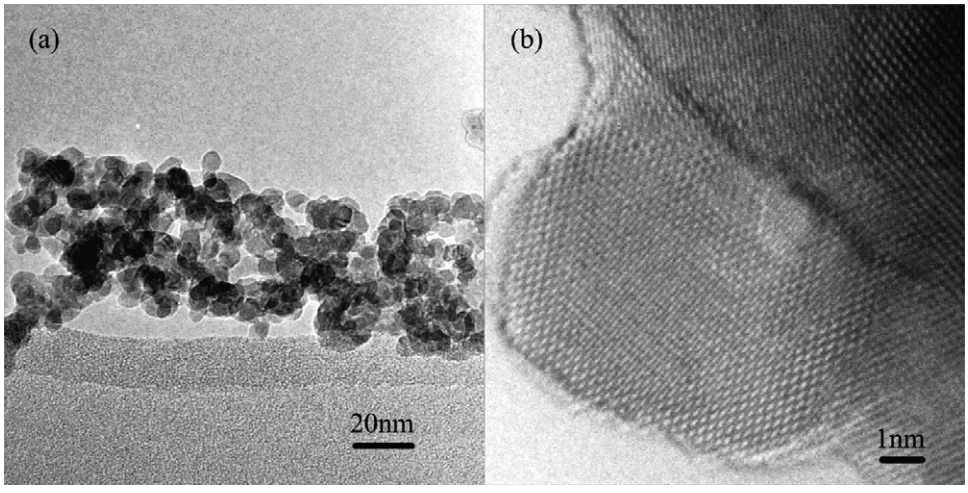

Fig. 2. Lower magnification (a) and high-resolution (b) TEM image of ZnO QDs.

From above results, it can be obviously found that slight introduction of SDS actually decreased the grain size and prompted the formation of ZnO QDs. In our system, the growth mechanism can be expressed as follows: as $ZnCl_2$ was added into the mixed solution of NH_4HCO_3 and SDS drop by drop, the white precipitations of $Zn_2(OH)_2CO_3$ gradually formed in the solution. During the annealing process, both $Zn_2(OH)_2CO_3$ and SDS decomposed. Because of the introduction of anionic surfactant SDS, the $Zn_2(OH)_2CO_3$ precipitations were surrounded by them. That is to say, the particles of $Zn_2(OH)_2CO_3$ cannot touch each other. As a result, the singly formed ZnO particles cannot become bigger without help of the other ZnO particles during the annealing process.

Raman scattering is very sensitive to the microstructure of nano-sized materials. It is a non-destructive characterization method for studying vibrational properties of ZnO nanostructures. Raman scattering was used here to clarify the quality and structure of ZnO QDs. Wurtzite ZnO belongs to C^4 ($P63mc$) space group, with two formula units per primitive cell. At the point of the Brillouin zone, group theory predicts the existence of the following phonon modes: $\Gamma = 2A_1 + 2B_1 + 2E_1 + 2E_2$. Among these modes, there are acoustic modes with $\Gamma_{aco} = A_1 + E_1$ and optical modes with $\Gamma_{opt} = A_1 + 2B_1 + E_1 + 2E_2$. For optical modes, B_1 modes are Raman silent modes. For the long-range electrostatic forces, both A_1 and E_1 modes are polar and are split into transverse (TO) and longitudinal optical (LO) phonons. Nonpolar phonon modes with symmetry E_2 have two frequencies, $E_2(H)$ is associated with oxygen atoms and $E_2(L)$ is associated with Zn sublattice. For ZnO single crystal materials, among the eight sets of optical modes, A_1, E_1, and E_2 are Raman active.

Fig. 3(a) shows the Raman spectrum of ZnO QDs. The peaks located at 336, 438 and 558 cm^{-1} can be observed. The band at 336 and 558 cm^{-1} can be assigned to $E_2(H)$–$E_2(L)$ and A_1(LO) mode, respectively. The peak at 438 cm^{-1} corresponds to the $E_2(H)$ mode, typical to the hexagonal phase of ZnO [20,21]. In order to analyze the Raman spectrum of ZnO QDs in details, a broad asymmetrical peak located at the wave-number region from 350 to 470 cm^{-1} was fitted with Gaussian functions, which was shown in Fig. 3(b). Four Gaussian curves were extracted for the spectrum (see the thin line curves), and their position was corresponding to 438, 426, 411 and 386 cm^{-1}, respectively. All peaks can be assigned on the basis of group theoretical analysis. The peak positions as well as comparison with the previous work of ZnO nanoparticles were listed in Table 1, from which a good agreement is evident. The Raman results indicated that the ZnO QDs keep the overall crystal structure of the bulk ZnO.

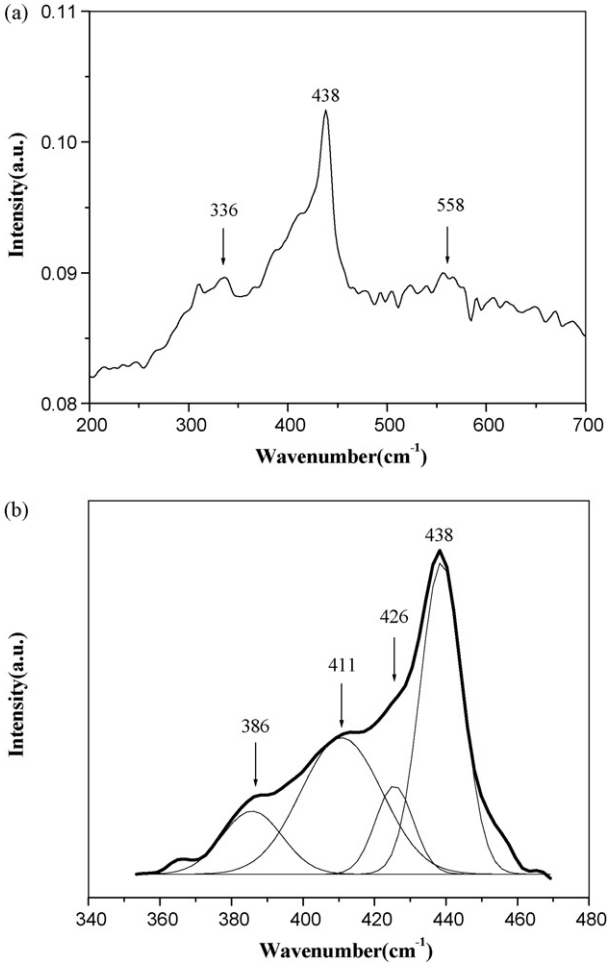

Fig. 3. Raman spectrum of ZnO QDs.

Table 1
Assignments of the observed Raman peaks for ZnO QDs sample

Peak (cm^{-1}) (present work)	Assignment	Peak (cm^{-1}) (nanoparticles Ref. [20,21])
336	$E_2(H)$–$E_2(L)$	332
386	A_1(TO)	389
411	E_1(TO)	418
426	E_{1T}	429
438	$E_2(H)$	439
558	A_1(LO)	559

The A_1(TO), E_1(TO), $E_2(H)$ and A_1(LO) mode showed 3, 7, 1 and 1 cm^{-1} redshift, respectively, compared with the value for nanoparticles of 25 nm in Ref. [20], which was carried out with the same laser source in the measurement. Usually, only optical phonon confinement is invoked as an explanation of the phonon frequency shifts in ZnO nanostructures [22]. However, Alim et al. [5,23] clarified the origin of the phonon peak shifts in ZnO QDs in their works recently. They reported that there are three main mechanisms that can induce phonon peak shifts in ZnO nanostructures: (i) spatial confinement within the dot boundaries; (ii) phonon localization by defects (oxygen deficiency, zinc excess, surface impurities, etc.); or (iii) laser-induced heating in nanostructure ensembles. While the first two factors were found to result in phonon peak shifts of few cm^{-1}, the third factor, laser-induced heating, could result in the Raman peak redshift as large as tens of cm^{-1}. In our Raman measurement, the laser source with long wavelength of 1064 nm was used so that the sample was prone to absorb heat during the process of measurement. In order to avoid this effect, the sample was measured for only 5 min under 100 mW. Therefore, only few cm^{-1} redshift happened in our results, which indicated both spatial confinement within the dot boundaries and phonon localization

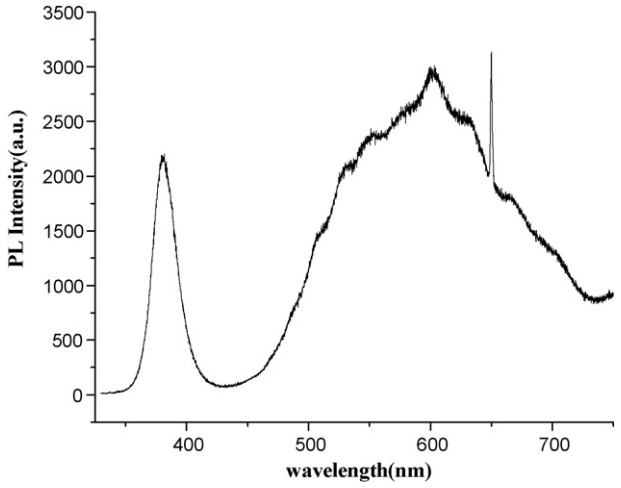

Fig. 4. Room-temperature PL spectrum of ZnO QDs.

by defects are the mainly reason for the redshift of the Raman scatter peaks.

Fig. 4 illustrates the room-temperature photoluminescence spectra of ZnO QDs to characterize the optical properties. Fig. 4 shows the PL spectrum consists of a relatively weak UV peak at 385 nm and a deep level emission band having a broad feature in the range of 420–700 nm. The peak at 650 nm is the scattering emission peak of excitation source. The UV emission band could be related to a near band-edge transition of ZnO, namely, the recombination of free excitons through an exciton–exciton collision process [24]. The center of deep level emission band located at about 600 nm, which is corresponding to orange luminescence. A great deal of research has been reported on the origin of the defect emission from ZnO. Theoretical and experimental studies have shown [25–30] that the defect states in the ZnO nanoparticles can be of several types: neutral, singly or doubly charged Zn vacancies (V_{Zn}), neutral, singly or doubly charge charged oxygen vacancies (V_O), singly charged or neutral interstitial Zn (Zn_i), interstitial O (O_i), a complex of V_O with Zn_i (V_OZn_i), a complex of V_{Zn} with Zn_i ($V_{Zn}Zn_i$) and substitution of O on a Zn site (O_{Zn}). The deep level involved in the orange luminescence was attributed to the intrinsic defect of oxygen interstitials [30]. Whatever, the strong deep level emission band in the PL spectra indicated that the as-synthesized ZnO QDs had defects, which also testified the results of Raman and XRD.

4. Conclusion

ZnO QDs were fabricated at low temperature of 200 °C through thermal decomposition method with slight introduction of anionic surfactant SDS. The structure, growth mechanism, and optical properties of ZnO QDs were investigated by the methods of XRD, SEM, TEM, Raman and PL. Such a low-temperature growth of ZnO QDs may provide a possibility to large-scale fabrication with a relatively low cost. The effects of annealing process and other growth parameters on the structure and optical properties of ZnO QDs will be investigated in the future.

Acknowledgments

This work is supported by the National Natural Science Foundation of China (NNSFC, No. 60778040), the science and technology bureau of Jilin province (Item No. 20060518) and gifted youth program of Jilin province (Nos. 20060123 and 20070123).

References

[1] Z.L. Wang, J. Phys.: Condens. Matter 16 (2004) R829–R858.
[2] Z.W. Pan, Z.R. Dai, Z.L. Wang, Science 291 (2001) 1947–1949.
[3] M.H. Huang, S. Mao, H. Feick, et al., Science 292 (2001) 1897–1899.
[4] V.A. Fonoberov, A. Balandin, Appl. Phys. Lett. 85 (2004) 5971–5973.
[5] K.A. Alim, V.A. Fonoberov, A. Balandin, Appl. Phys. Lett. 86 (2005) 053103–053105.
[6] L. Guo, S. Yang, C. Yang, et al., Appl. Phys. Lett. 76 (2000) 2901–2903.
[7] F. Demangeot, V. Paillard, P.M. Chassaing, et al., Appl. Phys. Lett. 88 (2006) 071921–071923.
[8] H.J. Fan, A.S. Barnard, M. Zacharias, Appl. Phys. Lett. 90 (2007) 143116–143118.
[9] X. Wang, Q. Li, Z. Liu, J. Zhang, Z. Liu, R. Wang, Appl. Phys. Lett. 84 (2004) 4941–4943.
[10] T. Makino, C.H. Chia, N.T. Tuan, et al., Appl. Phys. Lett. 77 (2000) 975–977.
[11] J. Zhou, N.S. Xu, Z.L. Wang, Adv. Mater. 18 (2006) 2432–2435.
[12] B.L. Zhu, C.S. Xie, D.W. Zeng, et al., Mater. Chem. Phys. 89 (2005) 148–153.
[13] S.W. Kim, T. Kotani, M. Ueda, et al., Appl. Phys. Lett. 83 (2003) 3593–3595.
[14] S.W. Kim, M. Ueda, M. Funato, S. Fujita, S. Fujita, J. Appl. Phys. 97 (2005) 104316.
[15] K.K. Kim, N. Koguchi, Y.W. Ok, et al., Appl. Phys. Lett. 84 (2004) 3810–3812.
[16] J.K. Lee, C.R. Tewell, R.K. Schulze, et al., Appl. Phys. Lett. 86 (2005) 183111–183113.
[17] E.W. Seeling, B. Tang, A. Yamilov, et al., Mater. Chem. Phys. 80 (2003) 257–263.
[18] L. Madler, W.J. Stark, S.E. Pratsinis, J. Appl. Phys. 92 (2002) 6537–6540.
[19] H.P. Klug, L.E. Alexaander, X-ray Diffraction Procedure for Crystalline and Amorphous Materials, Wiley, New York, 1974, p. 662.
[20] G. Xiong, U. Pal, J. Garcia Serrano, J. Appl. Phys. 101 (2007) 024317.
[21] F. Decremps, J.P. Porres, A.M. Saitta, et al., Phys. Rev. B 65 (2002) 092101.
[22] M. Rajalakshmi, A.K. Arora, B.S. Bendre, et al., J. Appl. Phys. 87 (2000) 2445–2448.
[23] K.A. Alim, V.A. Fonoberov, M. Shamsa, et al., J. Appl. Phys. 97 (2005) 124313.
[24] Y.C. Kong, D.P. Yu, B. Zhang, et al., Appl. Phys. Lett. 78 (2001) 407–409.
[25] K. Vanheusden, W.L. Warren, C.H. Seager, et al., J. Appl. Phys. 79 (1996) 7983–7990.
[26] A.B. Djurisic, Y.H. Leung, Small 2 (2006) 944.
[27] B.X. Lin, Z.X. Fu, Y.B. Jia, Appl. Phys. Lett. 79 (2001) 943–945.
[28] P.S. Xu, Y.M. Sun, C.S. Shi, et al., Nucl. Instrum. Methods: Phys. Res. B 199 (2003) 286–290.
[29] A. van Dijken, J. Makkinje, A. Meijerink, J. Lumin. 92 (2001) 323–328.
[30] D. Li, Y.H. Leung, A.B. Djurisic, Z.T. Liu, et al., Appl. Phys. Lett. 85 (2004) 1601–1603.